

## Hadron Structure and Form Factors

---

**C. Alexandrou\***

*Department of Physics, University of Cyprus, P.O. Box 20537, 1678 Nicosia, Cyprus and  
Computation-based Science and Technology Research Center, Cyprus Institute, P.O. Box 27456,  
1645 Nicosia, Cyprus*  
E-mail: [alexand@ucy.ac.cy](mailto:alexand@ucy.ac.cy)

We review recent results on hadron form factors and nucleon generalized parton distributions obtained with dynamical lattice QCD simulations. We discuss lattice artifacts and open questions, and present the connection of lattice results to hadron structure and to the corresponding quantities measured in experiment.

*The XXVIII International Symposium on Lattice Field Theory, Lattice2010  
June 14-19, 2010  
Villasimius, Italy*

---

\*Speaker.

## 1. Introduction

Lattice QCD simulations are currently being performed with dynamical degenerate u- and d- quarks with a mass close to their physical value as well as the strange quark using a number of different discretization schemes with the most common being Wilson-improved, staggered and chiral fermions. Furthermore, simulations at several lattice spacings and volumes are becoming available enabling a comprehensive study of lattice artifacts. The masses of low-lying hadrons have been computed and extrapolated to the continuum limit using large enough lattice sizes to ensure that volume effects are small [1, 2]. These calculations show agreement with experiment and therefore pave the way for evaluating phenomenologically interesting quantities beyond these masses.

Several collaborations, using dynamical quarks with pion mass down to about 300 MeV, have calculated the pion electromagnetic (EM) form factor [3], which is obtained from the matrix element  $\langle \pi^+(p') | J_\mu | \pi^+(p) \rangle = (p_\mu + p'_\mu) F_\pi(q^2)$  where  $q^2 = (p' - p)^2 = -Q^2$ . Based on vector dominance, lattice data are fitted to the form  $F_\pi(Q^2) = (1 + \langle r^2 \rangle Q^2 / 6)^{-1}$  to extract the mean squared radius, which is shown in Fig. 1. As can be seen, there is an increase in the value of  $\langle r^2 \rangle$  for smaller pion masses  $m_\pi$ . An accurate extraction of  $\langle r^2 \rangle$  benefits from evaluating the form factor at small values of  $Q^2$  accomplished by using twisted boundary conditions (b.c.). In a recent calculation, ETMC combined twisted b.c. and the so called ‘one-end’ trick to incorporate the all-to-all propagator and improve statistics. Using simulations with two degenerate light quarks ( $N_f = 2$ ) at two lattice spacings and two volumes [4] allowed the assessment of cut-off and volume effects. Extrapolating lattice results on  $F_\pi$  obtained with pion masses in the range of 300 MeV to 500 MeV, using NNLO chiral perturbation theory (PT), one reproduces experiment, as can be seen in Fig. 2 [4].

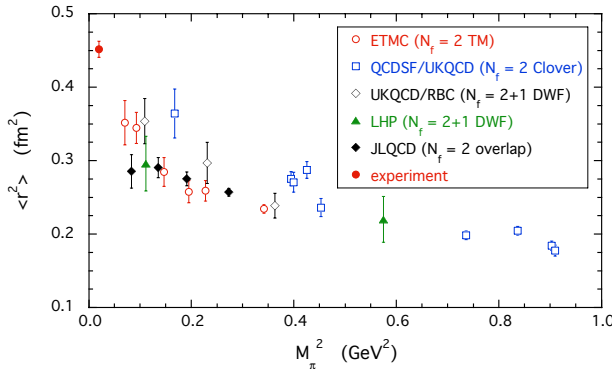


**Figure 1:** The pion mean square radius as a function of  $m_\pi^2$  obtained using simulations with  $N_f = 2$  twisted mass quarks.

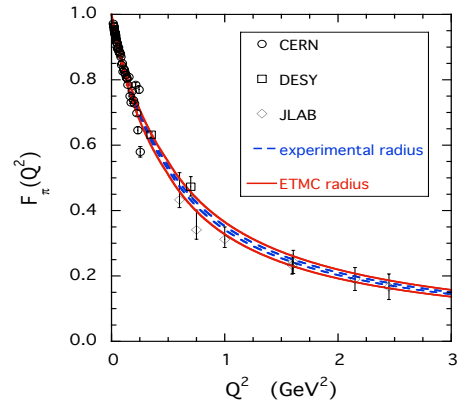


**Figure 2:**  $F_\pi$  extrapolated to the physical pion mass (red band) using NNLO chiral perturbation theory compared to experiment.

As simulations with quark masses close to the physical value become available study of resonances and decays of unstable particles become an important issue. The  $\rho$ -meson width has been studied by several groups [5]. Considering a  $\pi^+\pi^-$  system in the  $I = 1$ -channel, the P-wave scattering phase shift  $\delta_{11}(k)$  in infinite volume is related via Lüscher’s relation to the energy shift in a finite box. Using  $N_f = 2$  twisted mass fermions (TMF) and considering the center of mass frame

and two moving frames one extracts the phase shift at different values of the energy, shown in Fig. 3. From the effective range formula  $\tan\delta_{11}(k) = \frac{g_{\rho\pi\pi}^2}{6\pi} \frac{k^3}{E_{CM}(M_R^2 - E_{CM}^2)}$ , where  $k = \sqrt{E_{CM}^2/4 - m_\pi^2}$  one determines  $M_R$  and the coupling  $g_{\rho\pi\pi}$  and then extracts the width using  $\Gamma_\rho = \frac{g_{\rho\pi\pi}^2}{6\pi} \frac{k_R^3}{M_R^2}$ , where  $k_R = \sqrt{M_R^2/4 - m_\pi^2}$ . The results on the width as a function of  $m_\pi^2$  are shown in Fig. 4 [6].

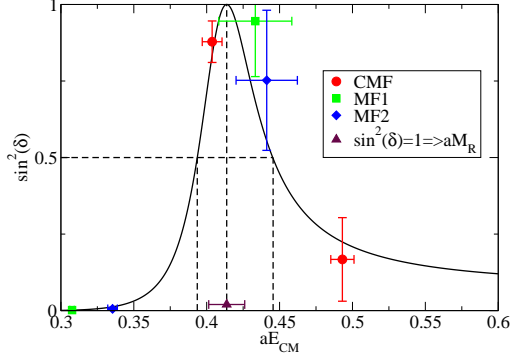


**Figure 3:** The  $\rho$ -meson phase shift at  $m_\pi = 308$  MeV for a lattice of  $L = 2.8$  fm.

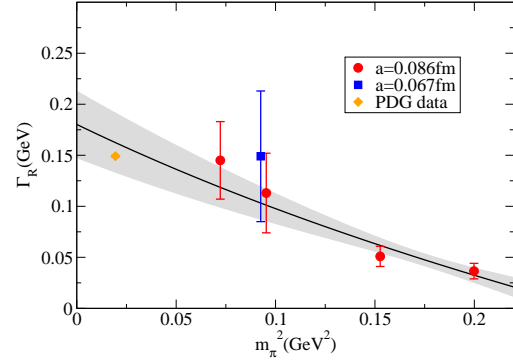


**Figure 4:** The  $\rho$ -meson width for  $N_f = 2$  twisted mass fermions as a function of  $m_\pi^2$ .

After the successful reproduction of the low-lying hadron masses [1, 2, 7, 8] one can address the masses of excited states of baryons using e.g. variational methods [9]. Furthermore, one can proceed with the evaluation of form factors (FFs) and generalized parton distributions (GPDs) that probe baryon structure. The characterization of nucleon structure is considered a milestone in hadronic physics and many experiments have been carried out to measure nucleon FFs and structure functions. Experiments on nucleon FFs started in the 50s. A new generation of experiments using polarized beams and targets are yielding high precision data spanning larger  $Q^2$  ranges. Therefore nucleon FFs can serve as a benchmark for lattice QCD. FFs provide ideal probes of the charge and magnetization of the hadron as well as a determination of its shape in analogy to similar studies in e.g. deuteron and other nuclei.

Non-relativistically the form factor can be related to the density distribution via

$$F(\vec{q}^2) = \int d^3x e^{-i\vec{q}\cdot\vec{x}} \langle \psi | \rho(\vec{x}) | \psi \rangle.$$

In Fig. 5 we show the intrinsic charge density contours of a spin-zero nucleus showing deformation revealed through measurements of transition densities using electron scattering.

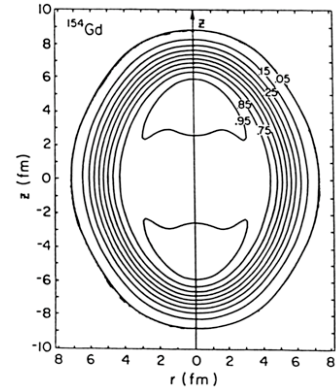


**Figure 5:** Tomographic view of the zero-spin deformed nucleus  $^{154}\text{Gd}$  derived from its rotational bands using electron scattering.

In what follows we will review the status of lattice QCD calculations on baryon form factors and nucleon generalized parton distributions.

## 2. Nucleon Generalized Parton Distributions - Definitions

In this section we define the quantities we will be presenting results on. High energy scattering can be formulated in terms of light-cone correlation functions. Considering one-particle states  $|p'\rangle$  and  $|p\rangle$ , GPDs are defined by [10, 11]:

$$F_{\Gamma}(x, \xi, q^2) = \frac{1}{2} \int \frac{d\lambda}{2\pi} e^{ix\lambda} \langle p' | \bar{\psi}(-\lambda n/2) \Gamma \mathcal{P} e^{ig \int_{-\lambda/2}^{\lambda/2} d\alpha n \cdot A(n\alpha)} \psi(\lambda n/2) | p \rangle,$$

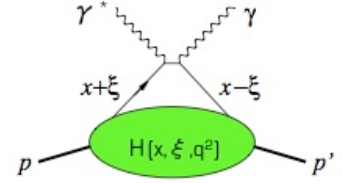
where  $\bar{P} = (p' + p)/2$ ,  $x$  and  $\xi$  are momentum fractions, and  $n$  is a light-cone vector with  $\bar{P} \cdot n = 1$ .

There are three different types of operators, depending on the choice of  $\Gamma$ : “Handbag” diagram

$$\Gamma = \not{n} \rightarrow \frac{1}{2} \bar{\psi}(p') \left[ \not{n} H(x, \xi, q^2) + i \frac{n_{\mu} q_{\nu} \sigma^{\mu\nu}}{2m} E(x, \xi, q^2) \right] \psi(p)$$

$$\Gamma = \not{n} \gamma_5 \rightarrow \frac{1}{2} \bar{\psi}(p') \left[ \not{n} \gamma_5 \tilde{H}(x, \xi, q^2) + \frac{n \cdot q \gamma_5}{2m} \tilde{E}(x, \xi, q^2) \right] \psi(p)$$

$$\Gamma = n_{\mu} \sigma^{\mu\nu} \rightarrow \text{tensor GPDs}$$



Expansion of the light cone operator leads to a tower of local twist-2 operators  $\mathcal{O}_{\Gamma}^{\mu_1 \dots \mu_n}$ , related to moments. The diagonal proton matrix elements  $\langle P | \mathcal{O}_{\Gamma}(x) | P \rangle$ , measured in deep inelastic scattering and connected to the parton distributions  $q(x)$ ,  $\Delta q(x)$ ,  $\delta q(x)$ , are defined by

$$\begin{aligned} \mathcal{O}_{\not{n}}^{\mu_1 \dots \mu_n} &= \bar{q} \gamma^{\{\mu_1} i D^{\mu_2} \dots i D^{\mu_n\}} q \xrightarrow{\text{unpolarized}} \langle x^n \rangle_q = \int_0^1 dx x^n [q(x) - (-1)^n \bar{q}(x)] \\ \tilde{\mathcal{O}}_{\not{n} \gamma_5}^{\mu_1 \dots \mu_n} &= \bar{q} \gamma_5 \gamma^{\{\mu_1} i D^{\mu_2} \dots i D^{\mu_n\}} q \xrightarrow{\text{helicity}} \langle x^n \rangle_{\Delta q} = \int_0^1 dx x^n [\Delta q(x) + (-1)^n \Delta \bar{q}(x)] \\ \mathcal{O}_{n_{\mu} \sigma^{\mu\nu}}^{\rho \mu_1 \dots \mu_n} &= \bar{q} \sigma^{\rho \{\mu_1} i D^{\mu_2} \dots i D^{\mu_n\}} q \xrightarrow{\text{transversity}} \langle x^n \rangle_{\delta q} = \int_0^1 dx x^n [\delta q(x) - (-1)^n \delta \bar{q}(x)] \end{aligned}$$

where  $q = q_{\downarrow} + q_{\uparrow}$ ,  $\Delta q = q_{\downarrow} - q_{\uparrow}$ ,  $\delta q = q_{\top} + q_{\perp}$ . The off-diagonal matrix elements extracted from deep virtual Compton scattering can be written in terms of generalized form factors (GFFs), which contain both form factors and parton distributions:

$$\begin{aligned} \langle N(p') | \mathcal{O}_{\not{n}}^{\mu_1 \dots \mu_n} | N(p) \rangle &= \bar{u}(p') \left[ \sum_{i=0, \text{even}}^{n-1} \left( A_{ni}(q^2) \gamma^{\{\mu_1} + B_{ni}(q^2) \frac{i \sigma^{\{\mu_1 \alpha} q_{\alpha}}{2m} \right) } q^{\mu_2} \dots q^{\mu_{i+1}} \bar{P}^{\mu_{i+2}} \dots \bar{P}^{\mu_n\}} \right. \\ &\quad \left. + \delta_{\text{even}}^n C_{n0}(q^2) \frac{1}{m} q^{\{\mu_1} \dots q^{\mu_n\}} \right] u(p) \end{aligned} \quad (2.1)$$

and similarly for  $\mathcal{O}_{\not{n} \gamma_5}$  in terms of  $\tilde{A}_{ni}(q^2)$ ,  $\tilde{B}_{ni}(q^2)$  and  $\mathcal{O}_{n_{\mu} \sigma^{\mu\nu}}$  in terms of  $A_{ni}^T$ ,  $B_{ni}^T$ ,  $C_{ni}^T$  and  $D_{ni}^T$ . We list the following special cases:

- $n = 1$ : Ordinary nucleon form factors:

$$\begin{aligned} A_{10}(q^2) = F_1(q^2) &= \int_{-1}^1 dx H(x, \xi, q^2), & B_{10}(q^2) = F_2(q^2) &= \int_{-1}^1 dx E(x, \xi, q^2) \\ \tilde{A}_{10}(q^2) = G_A(q^2) &= \int_{-1}^1 dx \tilde{H}(x, \xi, q^2), & \tilde{B}_{10}(q^2) = G_P(q^2) &= \int_{-1}^1 dx \tilde{E}(x, \xi, q^2), \end{aligned}$$

where in the case of the EM current,  $j_\mu = \bar{\psi}(x)\gamma_\mu\psi(x)$ , the nucleon matrix element is written in the form  $\bar{\psi}(p') \left[ \gamma_\mu F_1(q^2) + \frac{i\sigma_{\mu\nu}q^\nu}{2m} F_2(q^2) \right] \psi(p)$ , where the Dirac  $F_1$  and Pauli  $F_2$  FFs are related to the electric and magnetic Sachs FFs with the relations:  $G_E(q^2) = F_1(q^2) - \frac{q^2}{(2m)^2} F_2(q^2)$  and  $G_M(q^2) = F_1(q^2) + F_2(q^2)$ . For the axial vector current  $A_\mu^a = \bar{\psi}(x)\gamma_\mu\gamma_5\frac{\tau^a}{2}\psi(x)$  the nucleon matrix element is given by  $i\bar{\psi}(p') \left[ \gamma_\mu\gamma_5 G_A(q^2) + \frac{q^\mu\gamma_5}{2m} G_P(q^2) \right] \frac{\tau^a}{2}\psi(p)$ .

•  $A_{n0}(0), \tilde{A}_{n0}(0), A_{n0}^T(0)$  are moments of parton distributions, e.g.  $\langle x \rangle_q = A_{20}(0)$  and  $\langle x \rangle_{\Delta q} = \tilde{A}_{20}(0)$  are the spin independent and helicity distributions. Knowing these quantities one can evaluate the quark spin,  $J_q = \frac{1}{2}[A_{20}(0) + B_{20}(0)] = \frac{1}{2}\Delta\Sigma_q + L_q$  and investigate the fraction of the spin carried by quarks and its contribution to the total spin via the nucleon spin sum rule,  $\frac{1}{2} = \frac{1}{2}\Delta\Sigma_q + L_q + J_g$ , as well as the momentum fraction carried by gluons via the momentum sum rule:  $\langle x \rangle_g = 1 - A_{20}(0)$ .

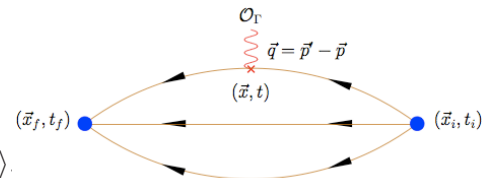
### 3. Lattice evaluation

In order to extract the matrix elements connected to GFFs we need to evaluate three-point correlators and compute the renormalization of the operators involved. Despite recent progress on the evaluation of disconnected loops most lattice calculations of GFFs do not take into account disconnected contributions. Therefore, in what follows, we consider iso-vector operators for which disconnected contributions are zero in the isospin limit. For one-derivative operators mixing with higher order operators is avoided by symmetrizing over the Lorentz indices and making them traceless. The study of cut-off and finite volume effects in a systematic way has just began for baryon GFFs. These are more difficult to assess since chiral expansions that described such dependencies are not as developed as in the light meson case. Having more uncertainties in the chiral expansion combined with the larger statistical noise, which for the two-point functions increases like  $\frac{\text{signal}}{\text{noise}} \sim \sqrt{N}e^{-(M_B - 3m_\pi/2)}$ , make the extrapolation of these quantities to the physical point much more demanding. In this review we will focus on: i) Nucleon form factors and lower moments using dynamical simulations with pion mass  $m_\pi \lesssim 500$  MeV and spatial lattice length  $L \gtrsim 2$  fm and ii) N- $\Delta$  system in order to determine the complete set of coupling constants needed in chiral expansions. Other topics relevant to hadron structure such as the strange nucleon FFs, hyperon, Roper and nucleon negative parity FFs, distribution amplitudes and transverse momentum dependent parton distribution functions can be found in Ref. [12] and in contributions to this volume.

• **Three-point functions:** For the extraction of matrix elements of local operators we need the evaluation of two-point and three-point functions defined by

$$G(\vec{p}, t) = \sum_{\vec{x}_f} e^{-i\vec{x}_f \cdot \vec{p}} \Gamma_{\beta\alpha}^4 \langle J_\alpha(\vec{x}_f, t_f) \bar{J}_\beta(0) \rangle$$

$$G^{\mu\nu}(\Gamma, \vec{p}', \vec{q}, t) = \sum_{\vec{x}_f, \vec{x}} e^{i\vec{x} \cdot \vec{q}} e^{-i\vec{x}_f \cdot \vec{p}'} \Gamma_{\beta\alpha} \langle J_\alpha(\vec{x}_f, t_f) \mathcal{O}^{\mu\nu}(\vec{x}, t) \bar{J}_\beta(0) \rangle.$$



Only the displayed connected diagram is evaluated, which, for most current applications, is done by using sequential inversion “through the sink” fixing the sink-source separation  $t_f - t_i$ , final momentum  $\vec{p}'$  and  $\Gamma$ - projection matrices. Smearing techniques are crucial for improving ground state dominance in three-point correlators and thus keep  $t_f - t_i$  as short as possible. We stress that it is important to ensure that the time separation  $t_f - t_i$  used is sufficiently large by performing the

calculation at a bigger time separation and checking the consistency of the results. The generalized eigenvalue method can further improve identification of the ground state [13] and enlarge the upper range of accessible  $Q^2$ -values [14].

• **Renormalization constants:** Most collaborations use non-perturbative renormalization. Using a momentum dependent source [15] one evaluates

$$S^u(p) = \frac{a^8}{V} \sum_{x,y} e^{-ip(x-y)} \langle u(x) \bar{u}(y) \rangle, \quad G(p) = \frac{a^{12}}{V} \sum_{x,y,z,z'} e^{-ip(x-y)} \langle u(x) \bar{u}(z) \mathcal{J}(z,z') d(z') \bar{d}(y) \rangle \quad (3.1)$$

with the amputated vertex functions given by  $\Gamma(p) = (S^u(p))^{-1} G(p) (S^d(p))^{-1}$ . The Z-factors can be determined in the RI'-MOM scheme by imposing the following conditions

$$Z_q = \frac{1}{12} \text{Tr}[(S(p))^{-1} S^{(0)}(p)] \Big|_{p^2=\mu^2}, \quad Z_q^{-1} Z_\sigma \frac{1}{12} \text{Tr}[\Gamma_{\mu\nu}(p) \Gamma_{\mu\nu}^{(0)-1}(p)] \Big|_{p^2=\mu^2} = 1, \quad (3.2)$$

to extract the renormalization factors  $Z_q$  and  $Z_\sigma$ . These conditions are imposed in the massless theory and therefore chiral extrapolations are needed. Doing the calculation at three values of the pion mass with  $N_f = 2$  TMF the mass dependence observed is very weak, as seen in Fig. 6 for the one-derivative axial and vector operators [16]. The corresponding results for  $Z_V$  and  $Z_A$  are shown in Fig. 7 where plateaux are improved after subtracting  $\mathcal{O}(a^2)$ -terms perturbatively [17]. Using the RI'-MOM scheme but with a momentum independent source, the RBC-UKQCD made a comparison between perturbative and non-perturbative determination of the renormalization constants and found that their results for  $\langle x \rangle_{u-d}$  [18] with perturbative renormalization are lower bringing them in agreement with LHPC's results, which used perturbative renormalization [19]. It is therefore important to compute the renormalization constants non-perturbatively.

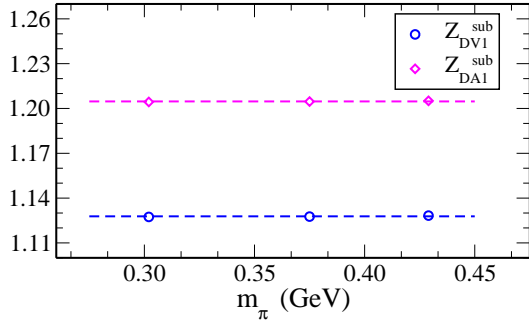


**Figure 6:** Mass dependence of the renormalization constant for vector and axial vector one-derivative operators for  $N_f = 2$  TMF [16].

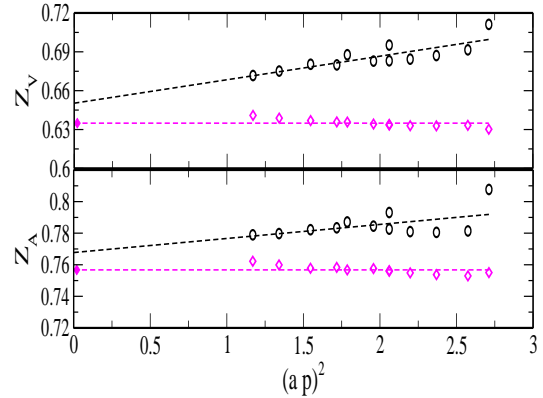


**Figure 7:**  $Z_V$  and  $Z_A$  with perturbative subtraction of  $\mathcal{O}(a^2)$ -terms for  $N_f = 2$  TMF [17].

• **Cut-off effects:** The nucleon axial charge  $g_A$ , the isovector momentum fraction  $\langle x \rangle_{u-d} = A_{20}(0)$  and helicity fraction  $\langle x \rangle_{\Delta u - \Delta d} = \tilde{A}_{20}(0)$  are calculated directly at  $Q^2 = 0$  requiring no fits. We can examine their dependence on the lattice spacing by obtaining these quantities at a given value of the pseudoscalar mass in units of  $r_0$ . In Fig. 8 we show results at three lattice spacings using  $N_f = 2$  TMF. As can be seen,  $\mathcal{O}(a^2)$ -terms are small and, allowing a linear dependence, yields

consistent results to those obtained with a constant fit. This is also true for the nucleon isovector anomalous moment  $\kappa_v$ , Dirac and Pauli radii  $r_1^2$  and  $r_2^2$  that require fits to the EM form factors.

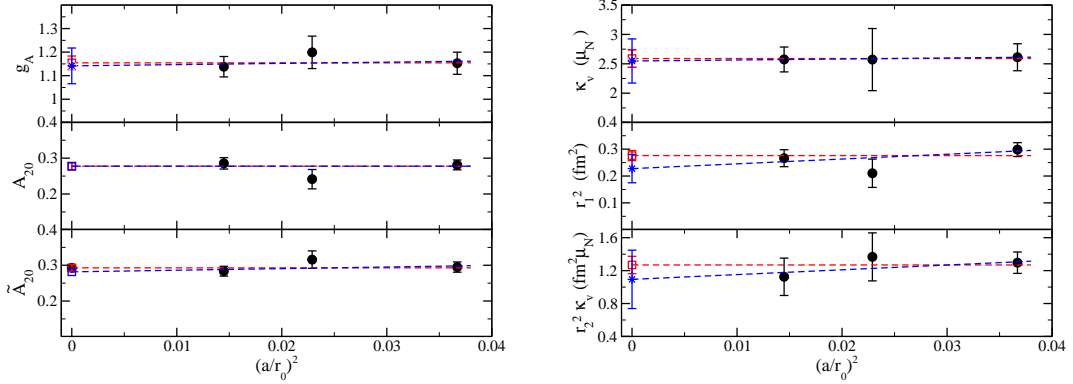


**Figure 8:** Right:  $g_A$ ,  $\langle x \rangle_{u-d}$ , and  $\langle x \rangle_{\Delta u-\Delta d}$ ; Left: the nucleon anomalous magnetic moment  $\kappa_v$ , the Dirac radius  $r_1^2$  and Pauli radius  $r_2^2$  times  $\kappa_v$  as a function of  $(a/r_0)^2$ . The red line is the result of fitting to a constant; the blue is a linear fit. The results are obtained using  $N_f = 2$  TMF [20].

We therefore conclude that cut-off effects are small for  $a < 0.1$  fm for  $\mathcal{O}(a)$ -improved actions and that we can use continuum chiral perturbation theory results to extrapolate to the continuum limit.

• **Finite volume corrections:** In Fig. 9 we compare results on  $g_A$ ,  $\langle x \rangle_{u-d}$  and  $\langle x \rangle_{\Delta u-\Delta d}$  computed on different lattice sizes as a function of  $m_\pi^2$ .

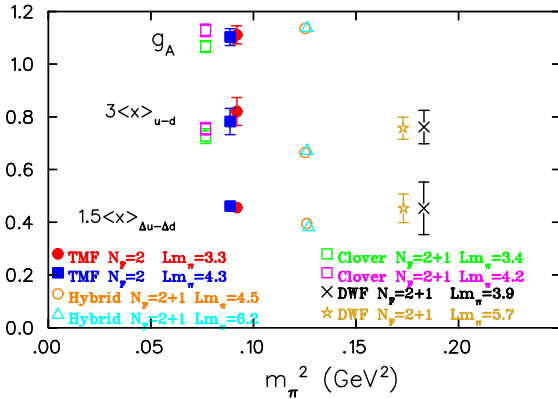


**Figure 9:**  $g_A$ ,  $3\langle x \rangle_{u-d}$  and  $\frac{3}{2}\langle x \rangle_{\Delta u-\Delta d}$  using TMF [20], Clover [21], hybrid [19] and DWF [18].

The observations are: i) Accurate lattice data by LHPC using domain wall valence quarks on staggered sea (hybrid) for  $m_\pi \sim 350$  MeV with  $Lm_\pi = 4.5$  and  $Lm_\pi = 6.2$  show no volume effects; ii) TMF results for  $m_\pi \sim 300$  MeV with  $Lm_\pi = 3.3$  and  $Lm_\pi = 4.3$  are consistent; iii) Results for  $\langle x \rangle_{u-d}$  using Clover fermions from QCDSF for  $m_\pi \sim 270$  MeV with  $Lm_\pi = 3.4$  and  $Lm_\pi = 4.2$  are consistent, whereas the values for  $g_A$  differ by about a standard deviation. iv) RBC-UKQCD results with domain wall fermions (DWF) with  $Lm_\pi = 3.9$  and  $Lm_\pi = 5.7$  show no volume effects for  $\langle x \rangle_{u-d}$  and  $\langle x \rangle_{\Delta u-\Delta d}$  [18].

Within the current statistical uncertainties this comparison, therefore shows that volume effects on  $\langle x \rangle_{u-d}$  and  $\langle x \rangle_{\Delta u-\Delta d}$  are negligible for  $Lm_\pi \gtrsim 3.3$ . For  $g_A$  volume effects of about one-standard deviation are seen for  $Lm_\pi \sim 3.4$  and pion mass below 300 MeV and therefore larger lattices keeping  $Lm_\pi \gtrsim 4$  maybe needed.

Comparing the isovector nucleon EM FFs as a function of  $Q^2$  at  $m_\pi \sim 300$  MeV we also find consistent results for  $Lm_\pi = 3.3$  and  $Lm_\pi = 4.3$ . A similar behavior is also observed for the nucleon axial FF  $G_A(Q^2)$  whereas the induced pseudoscalar FF  $G_p(Q^2)$ , which has a pion pole behavior, may suffer from larger finite volume corrections at low  $Q^2$ -values [22].



#### 4. Results on nucleon form factors

Having examined cut-off and volume effects we compare results from various collaborations computed with dynamical fermions for  $a \lesssim 0.1 \text{ fm}^1$  and  $Lm_\pi \gtrsim 3.3$ .

• **Nucleon axial charge:** The axial charge is well known experimentally. Since it is determined at  $Q^2 = 0$  there is no ambiguity associated with fitting the  $Q^2$ -dependence of the FF. In Fig. 10 we show recent lattice results using TMF and DWF as well as using a hybrid action of DWF on a staggered sea all of which are renormalized with  $Z_A$  computed non-perturbatively. As can be seen, there is a nice agreement among different lattice discretizations and no significant dependence on the quark mass down to about  $m_\pi = 260 \text{ MeV}$ .

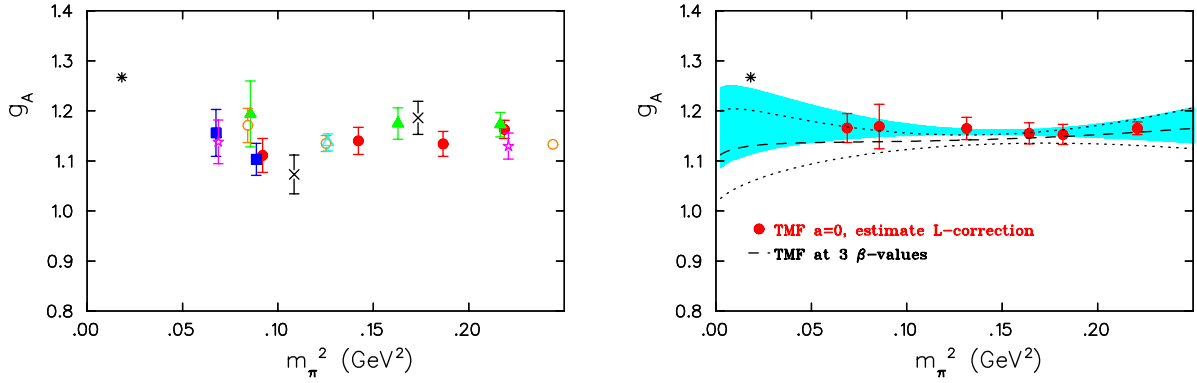


**Figure 10:** Left: Lattice data on  $g_A$  using  $N_f = 2$  TMF [20] ( $a = 0.089 \text{ fm}$ : filled red circles for  $L = 2.1 \text{ fm}$  and filled blue squares for  $L = 2.8 \text{ fm}$ ;  $a = 0.070 \text{ fm}$ : filled green triangles for  $L = 2.2 \text{ fm}$ ;  $a = 0.056 \text{ fm}$ : purple star for  $L = 2.7 \text{ fm}$  and open yellow square for  $L = 1.8 \text{ fm}$ ),  $N_f = 2 + 1$  DWF [23] (crosses for  $a = 0.114 \text{ fm}$  and  $L = 2.7 \text{ fm}$ ) and  $N_f = 2 + 1$  using DWF and staggered sea [19] ( $a = 0.124 \text{ fm}$ : open orange circles for  $L = 2.5 \text{ fm}$  and open cyan triangle for  $L = 3.5 \text{ fm}$ ). The physical point is shown by the asterisk. Right: Volume corrected TMF results extrapolated to the continuum limit together with the fit using HB $\chi$ PT (blue band). The band bounded by the lines is the resulting fit to the TMF data shown on the left.

To illustrate the size of lattice artifacts and obtain a value of  $g_A$  at the physical point, we use TMF results [22]. The volume corrected [24] data are extrapolated to  $a = 0$  using three lattice spacings, namely  $a = 0.089 \text{ fm}$ ,  $0.070 \text{ fm}$  and  $0.056 \text{ fm}$ , at two values of the pseudoscalar mass, by fitting to a constant. For intermediate masses we use data at the two coarser lattices. The continuum volume-corrected results are shown in Fig. 10. Chiral extrapolation using one-loop heavy baryon chiral perturbation theory (HB $\chi$ PT) with three fit parameters in the small scale expansion (SSE) [25] produces a value of  $g_A = 1.12(8)$  at the physical point, which is lower than the experimental value by about a standard deviation. The large error is due to the large correlation between the  $\Delta$  axial charge  $g_{\Delta\Delta}$  and the counter-term involved in the fit. Therefore, a lattice determination of  $g_{\Delta\Delta}$  will allow a more controlled chiral extrapolation. Fitting the raw lattice data produces the band shown by the dotted lines. Therefore one observes that, although the continuum volume-corrected results are closer to experiment, the largest uncertainty is due to the chiral extrapolation and at the physical point the values obtained using the raw and continuum volume-corrected lattice data are consistent.

<sup>1</sup>We note that results by the LHPC using a hybrid action have  $a = 0.124 \text{ fm}$ .



• **Nucleon form factors:** Recent lattice results on the EM isovector and axial FFs are shown in Fig. 11. We observe a nice agreement among lattice results, in particular for  $G_E(Q^2)$  and  $G_A(Q^2)$ . However, both  $G_E(Q^2)$  and  $G_A(Q^2)$  decrease with  $Q^2$  less rapidly than experiment. We note that a good description of the  $Q^2$ –dependence for both  $G_E(Q^2)$  and  $G_M(Q^2)$  is provided by a dipole form using the lattice-computed  $\rho$ –meson mass. Lattice results on  $G_p(Q^2)$  using TMF are not in agreement with results obtained with the hybrid action on a larger volume, in particular at small  $Q^2$  where  $G_p(Q^2)$  increases rapidly due to the pion-pole behavior. From the observed quark mass dependence of  $G_p(Q^2)$  [22] the 50 MeV difference in the pion mass may not be sufficient to fully account for this discrepancy, which may indicate volume effects.

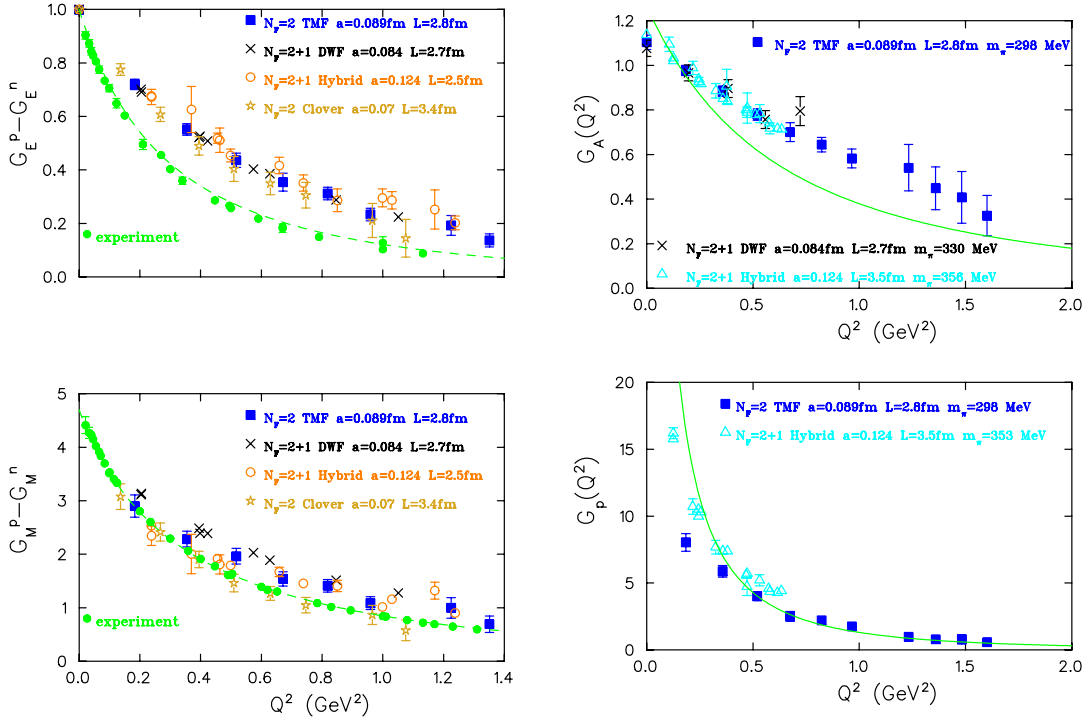


**Figure 11:** Left: Isovector electric and magnetic nucleon FFs at  $m_\pi \sim 300$  MeV using TMF [20] (filled blue squares) DWF [26] (crosses), hybrid [19] (open orange circles) and Clover [27] (yellow stars). Experimental data are shown with the filled green circles accompanied with Kelly’s parametrization shown with the dashed line. Right: Axial nucleon FFs. The solid line is a dipole fit to experimental data for  $G_A(Q^2)$  combined with pion pole dominance to get the solid curve shown for  $G_p(Q^2)$ .

Using HB $\chi$ PT to one-loop, with  $\Delta$  degrees of freedom and iso-vector  $N\Delta$  coupling included in LO [28] we perform a fit to  $F_1(m_\pi, Q^2)$  and  $F_2(m_\pi, Q^2)$  with five parameters, namely the iso-vector magnetic moment at the chiral limit  $\kappa_v^0$ , the isovector and axial N to  $\Delta$  coupling constants and two counterterms. As can be seen, the chiral extrapolation increases the value of  $F_1$  and  $F_2$  at low  $Q^2$  bringing it into qualitative agreement with experiment. Application of twisted b.c. with a study of the associated volume corrections [29] will be very useful in enabling us to obtain these FFs at lower  $Q^2$ -values permitting a better chiral extrapolation. Using the parameters extracted from the fits to  $F_1$  and  $F_2$  we obtain the chiral dependence of the isovector nucleon anomalous magnetic

moment and the Dirac and Pauli radii shown in Fig. 12.

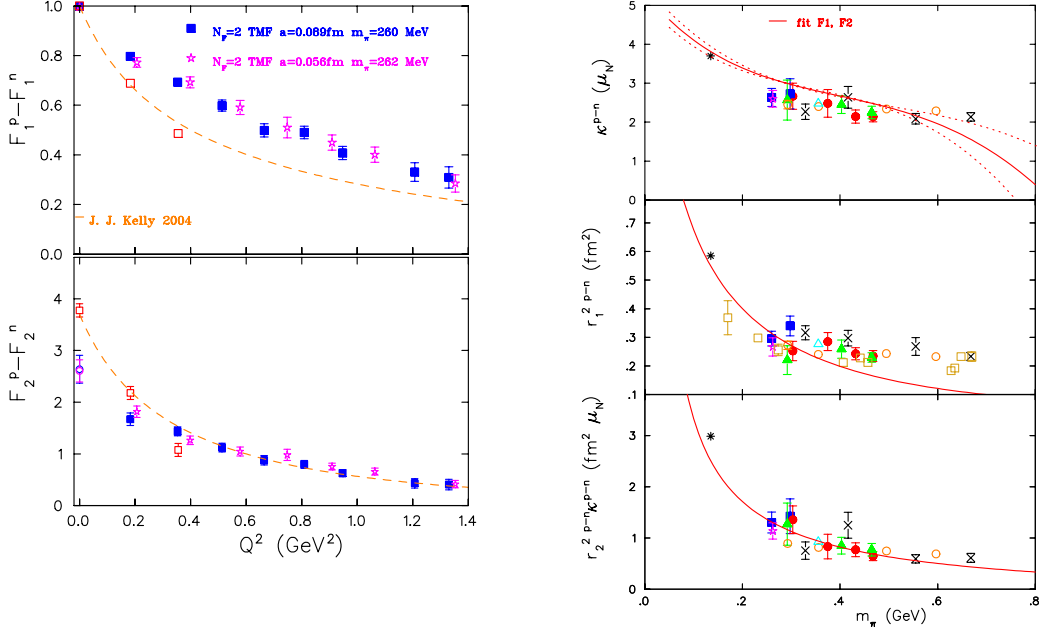


**Figure 12:** Left: Open squares show the chirally extrapolated results at the physical point. The dashed line is Kelly's parametrization of the experimental data. Right: The solid lines show the prediction of HB $\chi$ PT using the parameters obtained from fitting  $F_1(m_\pi, Q^2)$  and  $F_2(m_\pi, Q^2)$ . The notation is the same as that of Fig. 10. In addition, results for  $r_1^2$  [21] using Clover fermions are shown with the open squares.

## 5. Results on nucleon moments

In this section we show results on the nucleon matrix element of the one-derivative operators  $\bar{u}\gamma_{\{\mu}\overleftrightarrow{D}_{\nu\}}u - \bar{d}\gamma_{\{\mu}\overleftrightarrow{D}_{\nu\}}d$  and  $\bar{u}\gamma_5\gamma_{\{\mu}\overleftrightarrow{D}_{\nu\}}u - \bar{d}\gamma_5\gamma_{\{\mu}\overleftrightarrow{D}_{\nu\}}d$  in the  $\overline{MS}$  scheme at a scale  $\mu = 2$  GeV.

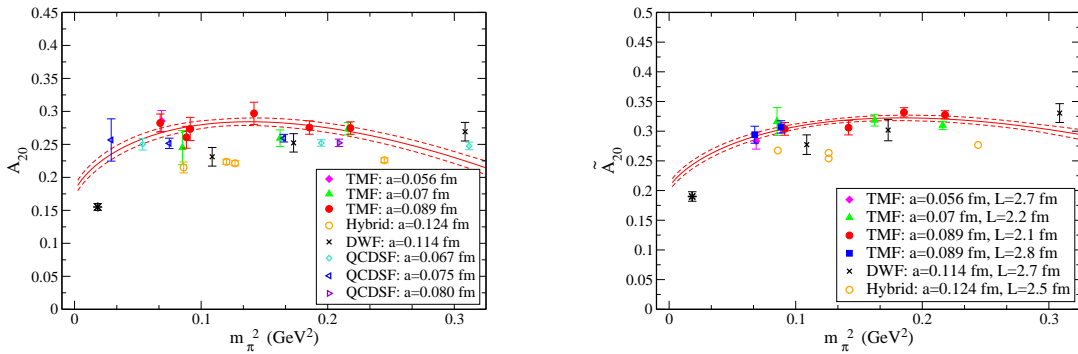


**Figure 13:** Recent results on  $\langle x \rangle_{u-d}$  and  $\langle x \rangle_{\Delta u - \Delta d}$ . The notation is the same as that of Fig. 10.

In Fig. 13 we compare recent results from ETMC [30], RBC-UKQCD [18], QCDSF [21] and LHPC [19] on the spin-independent and helicity quark distributions. All collaborations except LHPC use non-perturbatively computed renormalization constants. The ETMC has, in addition,

subtracted  $\mathcal{O}(a^2)$  terms perturbatively to improve the determination of the renormalization constants [16]. There is a spread in the values of the lattice results. It was noted that taking a renormalization free ratio leads to a better agreement among lattice data with  $Lm_\pi > 4$  [31]. In particular this brought the LHPC data in agreement with those from ETMC and QCDSF.

In HB $\chi$ PT [32] the expressions for the  $m_\pi$ -dependence of  $A_{20}$  and  $\tilde{A}_{20}$  are given by:

$$\langle x \rangle_{u-d} = C \left[ 1 - \frac{3g_A^2 + 1}{(4\pi f_\pi)^2} m_\pi^2 \ln \frac{m_\pi^2}{\lambda^2} \right] + \frac{c_8(\lambda^2) m_\pi^2}{(4\pi f_\pi)^2}, \quad \langle x \rangle_{\Delta u - \Delta d} = \tilde{C} \left[ 1 - \frac{2g_A^2 + 1}{(4\pi f_\pi)^2} m_\pi^2 \ln \frac{m_\pi^2}{\lambda^2} \right] + \frac{\tilde{c}_8(\lambda^2) m_\pi^2}{(4\pi f_\pi)^2}$$

Using  $\lambda^2 = 1 \text{ GeV}^2$  and the TMF results we obtain the curves shown in Fig. 13 which give a result higher than experiment for both observables. The very recent result by QCDSF [21] at  $m_\pi \sim 170 \text{ MeV}$  remains higher than experiment and highlights the need to understand such deviations.

## 6. N- $\Delta$ system

•  **$N\gamma^* \rightarrow \Delta$  form factors:** There is an extensive experimental program to study the  $N$  to  $\Delta$  EM transition and in particular to obtain accurate results on the sub-dominant quadrupole FFs  $G_{E2}^*(q^2)$  and  $G_{C2}^*(q^2)$  that probe deformation. The experimental results, shown in Fig. 14, are compatible with the blue band obtained assuming deformation in the N/ $\Delta$  and incompatible with the red band that includes no deformation. These FFs can be computed within lattice QCD and since no disconnected contributions are involved they provide yet other benchmark for lattice methods. The matrix element for  $N$  to  $\Delta$  EM transition is written in terms of three Sachs FFs as:

$$\langle \Delta(p', s') | j_\mu | N(p, s) \rangle = i\mathcal{A} \bar{\psi}_\sigma(p', s') \left[ G_{M1}^*(q^2) K_{M1}^{\sigma\mu} + G_{E2}^*(q^2) K_{E2}^{\sigma\mu} + G_{C2}^*(q^2) K_{C2}^{\sigma\mu} \right] \psi(p, s),$$

where  $\mathcal{A} = \sqrt{\frac{2}{3}} (m_N m_\Delta / E_\Delta(\vec{p}') E_N(\vec{p}))^{1/2}$  is a kinematical factor.

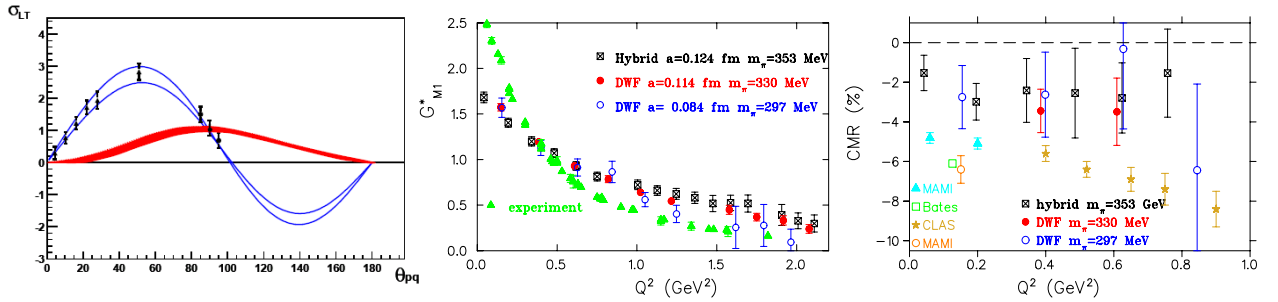


**Figure 14:**  $N$  to  $\Delta$  EM transition: Left: The transverse-longitudinal response function  $\sigma_{LT}$  vs c.m. angle between  $p$  and  $\gamma^*$  (from MAMI and Bates) [33]; Middle: The  $N$  to  $\Delta$  magnetic dipole FF; Right: The ratio of Coulomb quadrupole to magnetic dipole FF.

The extraction of the sub-dominant quadrupole FFs is done by constructing optimized sources that isolate  $G_{E2}^*$  and  $G_{C2}^*$  [34]. In Fig. 14 we show results using a hybrid action of DWF on staggered sea as well as  $N_f = 2 + 1$  DWF, provided by RBC-UKQCD. For the dominant dipole FF  $G_{M1}^*$ , like for the nucleon FFs, we observe a weaker  $Q^2$ -dependence as compared to experiment, that again

highlights the need of studying these FFS using simulations with  $m_\pi < 300$  MeV. Lattice results, shown in Fig. 14 for the ratio of the Coulomb quadrupole to the magnetic dipole FF are non-zero. This is also true for the electric quadrupole FF pointing to a deformation of the  $N/\Delta$ .

• **Weak  $N$  to  $\Delta$  transition:** In contrast to the EM transition, the weak  $N$  to  $\Delta$  is not well studied experimentally. Therefore a lattice determination of the axial  $N$  to  $\Delta$  FFs provide important input for phenomenology and in particular for chiral perturbation expansions. The weak  $N$  to  $\Delta$  matrix element  $\langle \Delta(p', s') | A_\mu^3 | N(p, s) \rangle = \bar{\psi}^\lambda(p', s') \mathcal{O}_{\lambda\mu} \psi(p, s)$  with

$$\mathcal{O}_{\lambda\mu} = i\mathcal{A} \left[ \left( \frac{C_3^A}{m_N} \gamma^\nu + \frac{C_4^A}{m_N^2} p'^\nu \right) (g_{\lambda\nu} g_{\rho\mu} - g_{\lambda\rho} g_{\mu\nu}) q^\rho + C_5^A g_{\lambda\mu} + \frac{C_6^A}{m_N^2} q_\lambda q_\mu \right]$$

where  $C_5^A$  is the equivalent of the nucleon  $G_A$  and  $C_6^A$  of the  $G_p$  showing a pion pole behavior [34]. In Fig. 15 we show results on the dominant FFs  $C_5^A$  and  $C_6^A$  obtained using a hybrid action of DWF on staggered sea at  $m_\pi \sim 350$  MeV and with  $N_f = 2 + 1$  DWF at  $m_\pi \sim 330$  MeV and  $m_\pi = 300$  MeV.

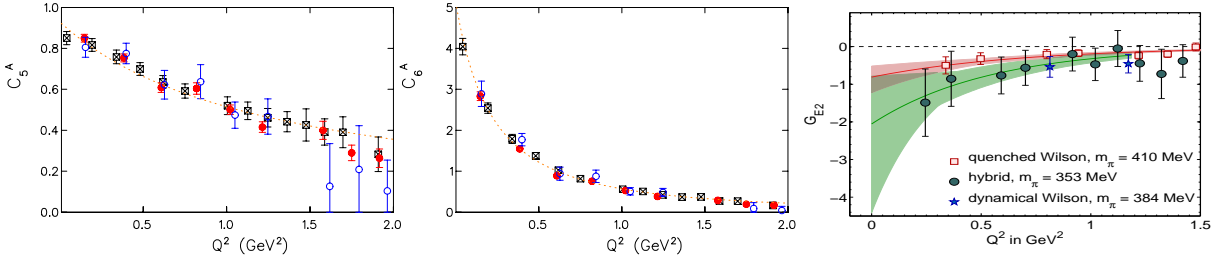


**Figure 15:** Left and middle: Axial  $N$  to  $\Delta$  FFs  $C_5^A$  and  $C_6^A$  respectively. The squares are for the hybrid action at  $m_\pi \sim 350$  MeV, the filled red circles for DWF at  $m_\pi \sim 330$  MeV and the open blue circles for DWF at  $m_\pi = 300$  MeV; Right:  $\Delta$  electric quadrupole FF for quenched,  $N_f = 2$  Wilson and  $N_f = 2 + 1$  hybrid action.

## 7. $\Delta$ electromagnetic form factors and structure

Experimentally the  $\Delta$  FFs are very difficult to measured due to the fact that the  $\Delta$  decays strongly. Only its magnetic moment is measured experimentally albeit with large errors. Therefore lattice calculations can complement experiment by providing these FFs.

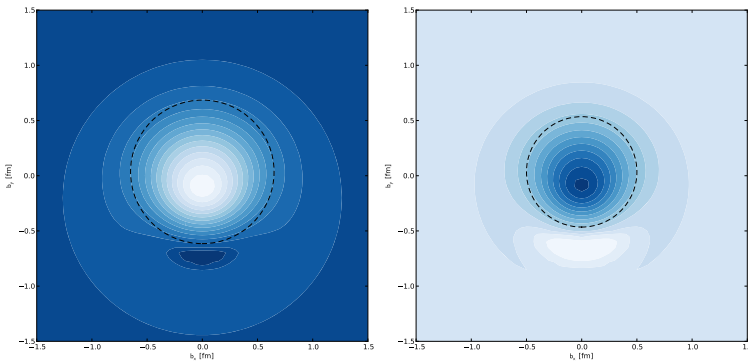


**Figure 16:** Quark transverse charge densities in the  $\Delta^{++}$  (left) and  $\Omega^-$  (right) for the  $3/2$ -spin projection along the  $x$ -axis. Darker colors denote smaller values and the charge of the particle is taken into account.

The matrix element  $\Delta(p', s') | j^\mu(0) | \Delta(p, s) \rangle = \bar{\psi}_\alpha(p', s') \mathcal{O}^{\alpha\mu\beta} \psi_\beta(p, s)$  can be written as

$$\mathcal{O}^{\alpha\mu\beta} = -\mathcal{A}_\Delta \left\{ \left[ F_1^*(Q^2) g^{\alpha\beta} + F_3^*(Q^2) \frac{q^\alpha q^\beta}{(2M_\Delta)^2} \right] \gamma^\mu + \left[ F_2^*(Q^2) g^{\alpha\beta} + F_4^*(Q^2) \frac{q^\alpha q^\beta}{(2M_\Delta)^2} \right] \frac{i\sigma^{\mu\nu} q_\nu}{2M_\Delta} \right\}$$

with e.g. the quadrupole FF given by:  $G_{E2} = (F_1^* - \tau F_2^*) - \frac{1}{2}(1 + \tau)(F_3^* - \tau F_4^*)$ , where  $\tau \equiv Q^2/(4M_\Delta^2)$ . Optimized sources are constructed to isolate the quadrupole FF  $G_{E2}$ , which probes deformation. The transverse charge density of a  $\Delta$  polarized along the x-axis can be defined in the infinite momentum frame. Using  $G_{E2}$  we can predict the ‘shape’ of  $\Delta$ . The result is shown in Fig. 16 and for spin projection 3/2 it is elongated along the spin axis. The  $\Omega^-$  shows a similar but smaller deformation [35]. The weak  $\Delta$  FFs can be computed in an analogous manner [36].

## 8. Conclusions

The nucleon EM form factors provide a benchmark for lattice QCD beyond hadron masses. Most collaborations obtain results for the isovector FFs up to about  $Q^2 = 2 \text{ GeV}^2$ . Systematic studies of lattice artifacts on GFFs are now under way and recent data reveal that cut-off effects are negligible for  $a \lesssim 0.1 \text{ fm}$ , whereas finite volume corrections, although difficult to evaluate, are within the current statistical errors of  $\sim (2 - 3)\%$  for  $Lm_\pi \gtrsim 3.3$ . A possible exception is  $G_p$  at low  $Q^2$ -values. We find that, in general, lattice results using different discretization schemes are consistent but they show a milder  $Q^2$ -dependence as compared to experiment. As illustrated in the case of the nucleon axial charge, the biggest uncertainty in comparing with experiment is the chiral extrapolation. Therefore a lattice determination of a number of couplings used as input in chiral extrapolations will enable global fits to e.g.  $N - \Delta$  system that can help extrapolation to the physical point. Interesting questions like for example the ‘shape’ of a hadron can be addressed using input from lattice form factors as demonstrated for the  $\Delta$  and  $\Omega$ . Moments of GPDs yield more detailed information on both longitudinal and transverse distributions and a tomography of hadron can be obtained by studying these quantities. We therefore conclude that overall there is good progress in baryon structure calculations and that we now are in an exciting era having simulations close enough to the physical point to begin to probe interesting dynamics in hadronic systems.

**Acknowledgments:** I would like to thank the members of the ETM collaboration and in particular M. Brinet, J. Carbonell, M. Constantinou, V. Drach, P. A. Harraud, K. Jansen, T. Korzec, M. Papinutto and O. Pene, my long-term collaborators G. Koutsou, J. W. Negele, and A. Tsapalis as well as Y. Proestos and M. Vanderhaeghen for their valuable input on the topics presented. This work was performed using HPC resources from GENCI (IDRIS and CINES) Grant 2009-052271, the Blue-Gene/P at JSC and was partly supported by funding received by the Cyprus Research Promotion Foundation under contracts EPYAN/0506/08, KY-Γ/0907/11/ and TECHNOLOGY/ΘΕΠΠΣ/0308(BE)/17.

## References

- [1] St. Dürr *et al.* (BMW), Science 322, 1224 (2008).
- [2] C. Alexandrou *et al.* (ETMC), Phys. Rev. D **80** 114503 (2009).
- [3] T. Kaneko *et al.* (JLQCD), PoS **LAT2007**, 148 (2007); A. Jüttner *et al.* (RBC-UKQCD), PoS C **D09** (2009) 010; D. Brömmel *et al.* (QCDSF/UKQCD) Eur. Phys. J. C **51**, 335 (2007); D. Brömmel *et al.* (QCDSF), Eur. Phys. J. C **51**, 335 (2007); F. D. R. Bonnet *et al.*, Phys. Rev. D. **72**, 054506 (2005).
- [4] R. Frezzotti, V. Lubicz and S. Simula, Phys. Rev. D **79**, 074506 (2009).

- [5] J. Frison *et al.*, arXiv:1011.3413; S. Aoki *et al.* (PACS-CS), arXiv:1011.1063; S. Aoki *et al.*, Phys. Rev. D **76**, 094506 (2007); M. Göckeler *et al.* (QCDSF), PoS **LATTICE2008**, 136 (2008).
- [6] X. Feng, K. Jansen and D. B. Renner, arXiv:0910.4871 [hep-lat].
- [7] A. Waker-Loud *et al.* (LHPC), Phys. Rev. D **79** 054502 (2009).
- [8] S. Aoki *et al.* (PACS-CS) Phys. Rev. D **79**, 034503 (2009).
- [9] J. M. Bulava *et al.*, Phys. Rev. D **79**, 034505 (2009); M. S. Mahbub *et al.* Phys. Lett. B **679**, 418 (2009); G. Engel, *et al.*, arXiv:0910.2802 [hep-lat].
- [10] M. Diehl, Phys. Rep. 388, 41 (2003).
- [11] X. Ji, J. Phys. G24, 1181 (1998).
- [12] J. M. Zanotti, PoS **LATTICE2008**, 007 (2008).
- [13] B. Blossier, M. Della Morte, G. von Hippel, T. Mendes and R. Sommer, JHEP **0904**, 094 (2009).
- [14] H.-W. Lin *et al.*, arXiv:1005.0799
- [15] M. Göckeler *et al.* (QCDSF), Nucl. Phys. **B544**, 699 (1999).
- [16] C. Alexandrou, M. Constantinou, T. Korzec, H. Panagopoulos and F. Stylianou, arXiv:1006.1920.
- [17] C. Alexandrou, M. Constantinou, T. Korzec, H. Panagopoulos and F. Stylianou, PoS **Lattice 2010**, 224 (2010); in preparation.
- [18] Y. Aoki *et al.* (RBC-UKQCD), Phys. Rev. D **82**, 014501 (2010).
- [19] J. D. Bratt *et al.* (LHPC), arXiv:1001.3620.
- [20] C. Alexandrou *et al.* (ETMC), PoS **LAT2009**, 145 (2009), arXiv:0910.3309.
- [21] J. Zanotti (QCDSF), private communication.
- [22] C. Alexandrou *et al.* (ETMC), in preparation.
- [23] T. Yamazaki *et al.* (RBC-UKQCD), Phys. Rev. D **79**, 114505 (2009).
- [24] A. Ali Khan, *et al.* (QCDSF), Phys. Rev. D **74**, 094508 (2006).
- [25] T. R. Hemmert, M. Procura and W. Weise, Phys. Rev. D **68**, 075009 (2003).
- [26] S. N. Syritsyn *et al.* (LHPC), Phys. Rev. D **81**, 034507 (2010).
- [27] H. Wittig (CLS), private communication.
- [28] T. R. Hemmert and W. Weise, Eur. Phys. J. A **15**, 487 (2002); M. Göckeler *et al.*, Phys. Rev. D **71**, 034508 (2005).
- [29] M. Göckeler *et al.* (QCDSF-UKQCD), PoS **LATTICE2008** 138 (2008).
- [30] C. Alexandrou *et al.* (ETMC), PoS **LAT2009**, 136 (2009); T. Korzec, private communication.
- [31] D. B. Renner, PoS **LAT2009** (2009), arXiv:1002.0925.
- [32] D. Arndt, M. Savage, Nucl. Phys. **A697**, 429 (2002); W. Detmold, W. Melnitchouk, A. Thomas, Phys. Rev. D **66**, 054501 (2002).
- [33] C. N. Papanicolas, Eur. Phys. J. A **18**, 141 (2003).
- [34] C. Alexandrou *et al.*, PoS **LAT2009**, 156 (2009), arXiv:0910.5617; C. Alexandrou, Th. Leontiou, J. W. Negele and A. Tsapalis, Phys. Rev. Lett. **98**, 052003 (2007).
- [35] C. Alexandrou *et al.*, Phys. Rev. D **79**, 014507 (2009); Nucl. Phys. **A825**, 115 (2009).
- [36] C. Alexandrou *et al.*, PoS **Lattice 2010**, 141 (2010), arXiv:1011.3233.